

Bioinspired, Tree-Root-Like Interfacial Designs for Structural Batteries with Enhanced Mechanical Properties

Tianwei Jin, Yirui Ma, Zechen Xiong, Xiaoyu Fan, Yu Luo, Zeyu Hui, Xi Chen, and Yuan Yang*

Structural batteries are attractive for weight reduction in vehicles, such as cars and airplanes, which requires batteries to have both excellent mechanical properties and electrochemical performance. This work develops a scalable and feasible tree-root-like lamination at the electrode/separator interface, which effectively transfers load between different layers of battery components and thus dramatically enhances the flexural modulus of pouch cells from 0.28 to 3.1 GPa. The underlying mechanism is also analyzed by finite element simulations. Meanwhile, the interfacial lamination has a limited effect on the electrochemical performance of Li-ion cells. A graphite/LiNi_{0.5}Mn_{0.3}Co_{0.2}O₂ full cell with such interfacial lamination delivers a steady discharge capacity of 148.6 mAh g⁻¹ at C/2 and 95.5% retention after 500 cycles. Moreover, the specific energy only decreases by 3%, which is the smallest reduction reported so far in structural batteries. A prototype of “electric wings” is also demonstrated, which allows an aircraft model to fly steadily. This work illustrates that engineering interfacial adhesion is an effective and scalable approach to develop structural batteries with excellent mechanical and electrochemical properties.

a multifunctional component in vehicles, which serves as both a power source and a structural component.^[10–13] Hence, the total vehicle weight is expected to be reduced due to the mass reduction of structural components, such as car frames and airplane wings.

This “structural battery” concept has drawn increasing attention in recent years, and it has been discussed by leading electric vehicle companies lately.^[14,15] The key requirement of structural batteries is enhanced mechanical properties, such as strength, modulus, and robustness under different kinds of mechanical deformation (e.g., shearing, flexing, compression, and tension). Strategies to enhance mechanical properties have been explored at both system and material levels. At the system level, cells were integrated with external supporting materials with high strength, such as metals and carbon fiber

(CF)-based fabric, to form better mechanical configurations like sandwich structures and strengthen the battery systems.^[16–18] However, this strategy inevitably results in lower energy densities because of the extra components for reinforcements, and reported reductions are in the range of 40–95%.^[16–18] At the material level, the underlying principle is to develop new multifunctional materials, which not only function as necessary components in a battery, but also provide enhanced mechanical properties. These materials range over all components in a battery, such as active electrode materials, electrolytes, binders, and substrates.^[19–22] For example, various groups demonstrated that carbon fibers, which have been widely used for load carrying, can serve as the anode itself or the cathode current collector for structural batteries.^[23–26] However, the cycling performance of carbon fibers is not satisfactory, and lithiation dramatically weakens the mechanical properties of carbon fibers.^[27,28] Moreover, it is difficult to integrate carbon fibers and cathode materials densely, so the cell energy density is severely compromised. Besides electrode materials, mechanically strong aramid fibers have been explored as the separator, which remarkably enhances both safety and tensile strength of structural batteries, but the cell's capacity and cycling stability are sacrificed considerably.^[29]


Among different mechanical properties to enhance, flexural properties are especially important, since bending is one of the most common mechanical deformations in cars and aircraft.

1. Introduction

Lightweighting is critical to enhancing the operational duration and performance of transportation vehicles.^[1–4] This demand is a major driving force for the development of batteries with high energy density, which has achieved significant progress in the last three decades, but becomes increasingly challenging nowadays.^[5,6] Batteries with high energy density are also prone to thermal runaway and mechanical damage,^[7–9] which requires protective components with extra weight. An alternative and potentially powerful solution is to use the battery as

T. Jin, Y. Ma, X. Fan, Y. Luo, Z. Hui, Prof. Y. Yang
Program of Materials Science and Engineering
Department of Applied Physics and Applied Mathematics
Columbia University
New York, NY 10027, USA
E-mail: yy2664@columbia.edu

Z. Xiong, Prof. X. Chen
Earth Engineering Center
Center for Advanced Materials for Energy and Environment
Department of Earth and Environmental Engineering
Columbia University
New York, NY 10027, USA

 The ORCID identification number(s) for the author(s) of this article can be found under <https://doi.org/10.1002/aenm.202100997>.

DOI: 10.1002/aenm.202100997

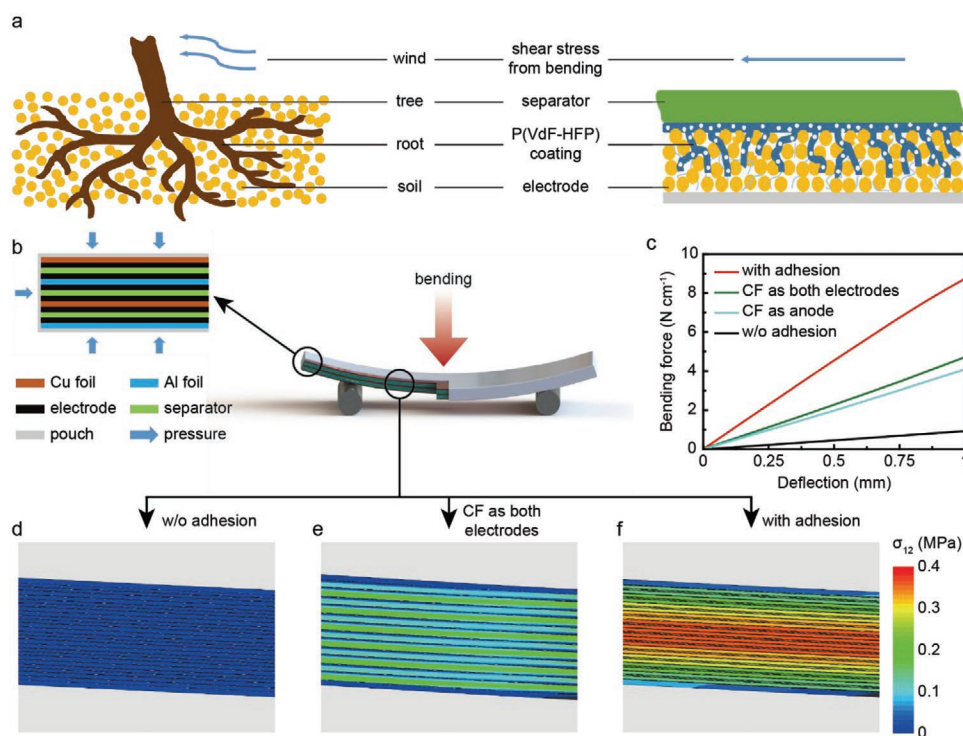


Figure 1. A schematic of the tree-root-inspired electrode/separator interfacial adhesion, and effects of mechanical properties of cell components and interfaces on the flexural performance of a full Li-ion cell. a) The analogy between a tree against strong wind (left) and the electrode/separator adhesion against shearing introduced by bending (right). b) The cell configuration under three-point bending in finite element (FE) simulation. For clarity, only three repeating graphite/NMC units are shown, and the thicknesses of all layers are drawn to be the same. c) The bending force per width–deflection curves of pouch cells within a deflection of 1 mm in FE simulation. “w/o adhesion” and “with adhesion” indicate a standard Li-ion cell without and with adhesion between electrodes and separators, respectively. “CF as anode” and “CF as both electrodes” are cells with the anode and both electrodes replaced by carbon fiber (CF), respectively. d–f) The simulated shear stress distributions of d) a standard Li-ion cell without adhesion between electrodes and separators, e) a cell with both anode and cathode replaced by CF, and f) a standard Li-ion cell with electrode/separator adhesion at a deflection of 1 mm. All cells are 2.1 mm thick and 7.0 cm long. More details can be found in the “FE Simulations” section in the Supporting Information.

Conventional Li-ion batteries have a low flexural modulus of ≈ 300 MPa, due to sliding between different component layers within. To address this challenge, Chang and co-workers developed a clever concept of using polymer “rivets” to interlock different layers to avoid their relative sliding, which enhances the flexural modulus to 1.5 GPa, similar to polypropylene.^[30] However, the overall energy density of these batteries is reduced by $\approx 40\%$ due to the introduction of those electrochemically inert parts and necessary redundancy in the margin of anode and separator to avoid shorting. This strategy also increases manufacturing challenges as it requires extra cutting and alignment of electrodes.

To hinder sliding between different layers inside a battery, we are inspired by how trees immobilize soil and themselves against strong wind (Figure 1a). The tree and the soil are analog to the separator and the granular electrode, respectively, and wind is equivalent to shear stress introduced by bending deformation. The success of trees’ mechanical stability originates from their deep and strong root networks, which hold soil firmly. Inspired by this structure, we developed a method to infiltrate polymeric binding materials into the porous cathode and anode, so that binders form a continuous network, followed by laminating them to a ceramic-coated separator by hot pressing (Figure 1a). As a result, the separator is bonded to the

powder-based electrode by a binder network like the tree root structure, which dramatically enhances the flexural properties of batteries. For example, the flexural modulus of a graphite/LiNi_{0.5}Mn_{0.3}Co_{0.2}O₂ (NMC532)-based Li-ion battery with commercial-level mass loading (≈ 3 mAh cm⁻² for a single layer) is enhanced by 11 times, from ≈ 281 MPa to ≈ 3.1 GPa, which is similar to epoxy. By finite element (FE) analysis, we also show that the flexural strength could be further enhanced by using alginate binder to strengthen the substrate/electrode adhesion.

Furthermore, since this strategy introduces limited redundant materials and space into a battery, the specific energy is only compromised by $\approx 3\%$. Further electrochemical characterizations show that such structural Li-ion cells can deliver a comparable specific capacity with conventional batteries, such as 148.6 mAh g⁻¹ at C/2 with a retention of 95.5% after 500 cycles. Such cycling performance and specific energy show that the proposed strategy does not cause noticeable side reactions or significantly affect the electrochemical performance. To further demonstrate practical application, we replaced the wings of an aircraft model with such tree-root-inspired structural batteries as the power source and the aircraft model flew steadily (Video S1, Supporting Information). In contrast, with conventional batteries, the aircraft model fell quickly since the wings deformed easily against airflow due to batteries’ poor

mechanical properties. This is the first demonstration with a battery as both the load-bearing component and the only power source in the aircraft, to the best of the authors' knowledge. This work demonstrates a scalable method to enhance flexural properties of structural batteries with little compromise on energy density.

2. Results and Discussions

2.1. Mechanical Simulations of Structural Batteries

As a battery consists of multiple layers stacked together, its flexural properties are determined by the mechanical properties of both the layers themselves and their interfaces. To understand their individual effects separately, we performed a quasistatic 2D plane-stress FE analysis on a three-point bending test of a Li-ion cell with multilayer stacking inside, with Figure 1b as an illustration. To mimic a real test, the cell in FE is 2.1 mm in thickness and 7 cm in length, which includes 11 layers of graphite anode and 11 layers of NMC cathode (33 mAh cm⁻² in total). The thicknesses of Cu foil, graphite anode, separator, NMC cathode, and Al foil are 9, 60, 20, 60, and 13 μm, respectively, where active materials are coated on both sides of the metal foils (see the Supporting Information for details). To balance accuracy and computational cost, we ensured that each component layer has at least two 4-node quadrilateral elements (CPS4R) in its thickness direction. The boundary and loading conditions in the FE simulation are the same as the three-point bending experiments in Figure S1c (Supporting Information), and a mesh convergence study is also conducted. The packaging layer and the atmospheric pressure are also considered in the simulation, which are critical to mimicking the real scenario. Details can be found in the Supporting Information.

Four cases were studied and their bending force–deflection curves are shown in Figure 1c. The baseline is with conventional battery materials and no binding between electrodes and separators. The electrode/separator interfaces are defined as frictional contact with a frictional coefficient of 0.4.^[31] Due to the external atmospheric pressure, the frictional force hinders the relative sliding between electrodes and separators, but this resistance is relatively small. Therefore, at a deflection of 1 mm, the simulated bending force per width and the equivalent flexural modulus (E_f) are only 0.92 N cm⁻¹ and 310 MPa, respectively. When the anode (both graphite and Cu) is replaced by stronger carbon fiber with a modulus of 230 GPa,^[28] the bending force and E_f , respectively, increase to 2.9 N cm⁻¹ and 979 MPa at the same level of deflection. If both electrodes are replaced by carbon fibers, the bending force and E_f only increase slightly to 4.1 N cm⁻¹ and 1.38 GPa, respectively. Such poor mechanical properties arise from the relative sliding of components about frictional interfaces, and thus all components deform about their own neutral axes with poor load transfer, leading to a large compromise in flexural properties of the whole cell. The poor load transfer between different layers is also reflected by the small and discontinuous shear stress in these cells (Figure 1d,e). Moreover, cell inflection near two supporting beams was observed in both simulation and experiment, which indicates relative sliding between components

(Figure S1d, Supporting Information). These results reveal that merely improving the mechanical properties of components without addressing the interfacial sliding issue is not enough to rigidify structural batteries.

On the other hand, if different components in a standard battery are bonded together as a laminate so that all components share a common neutral axis, load transfer will be more efficient, and tremendously higher flexural modulus and stiffness can be achieved. With a moderate interfacial adhesive energy of 0.2 N cm⁻¹ between an electrode and a separator, the bending force and E_f are remarkably enhanced to 8.8 N cm⁻¹ and 2.97 GPa, respectively, at a deflection of 1 mm (Figure 1c). Figure 1f further shows that the shear stress in such a laminated cell is much larger than that in a cell without adhesion (Figure 1d,e), suggesting higher E_f . Moreover, the continuity of stress through all cell components also affirms good mechanical integrity and satisfying load transfer. In addition, no inflection is observed near the supporting beams in both FE simulation and experiments (Figure S1e, Supporting Information), further demonstrating efficient load transfer. These results indicate that interfacial adhesion dominates the flexural modulus of a Li-ion cell, and it should be enhanced along with the mechanical properties of components themselves for realizing high-performance structural batteries. In addition, if the two strategies of enhancing interfacial adhesion and enhancing components' mechanical properties can be combined, the flexural performance should be further improved. For example, Asp et al. recently reported a combination of a polymer electrolyte and CF-based electrodes, where the semisolid polymer electrolyte allows load transfer between different layers, acting as effective interfacial adhesion.^[32] Such a combination should realize better flexural performance than using only one strategy above.

2.2. Battery Fabrication and Mechanical Properties

To realize strong adhesion between electrodes and separators in practice, we developed a tree-root-like, continuous binder network at the subsurface region of a granular electrode, which binds with a ceramic-coated separator tightly. Such a tree-root-like structure was realized by a phase inversion method, as illustrated in Figure 2a.^[33] First, poly(vinylidene fluoride-co-hexafluoropropylene) (P(VdF-HFP)) was dissolved in acetone with 10 wt% water as the nonsolvent. The as-prepared solution was cast onto an NMC or graphite electrode and permeated into the porous electrode (Step 1). Upon the evaporation of acetone and water in sequence, porous P(VdF-HFP) was formed continuously among electrode particles and on the electrode surface, as shown in Figure S1a (Supporting Information). The thickness of the extra P(VdF-HFP) coating on an electrode is 5–10 μm, which formed good adhesion to the polyvinylidene fluoride (PVdF)-Al₂O₃ composite coating on the separator during hot pressing (Step 2).

The permeation of P(VdF-HFP) into electrodes was validated by the cross-sectional energy dispersive spectroscopy (EDS) line scan through an as-coated graphite electrode with a sodium alginate binder (Figure 2b). The signal of fluorine, which only exists in P(VdF-HFP), concentrated on the electrode

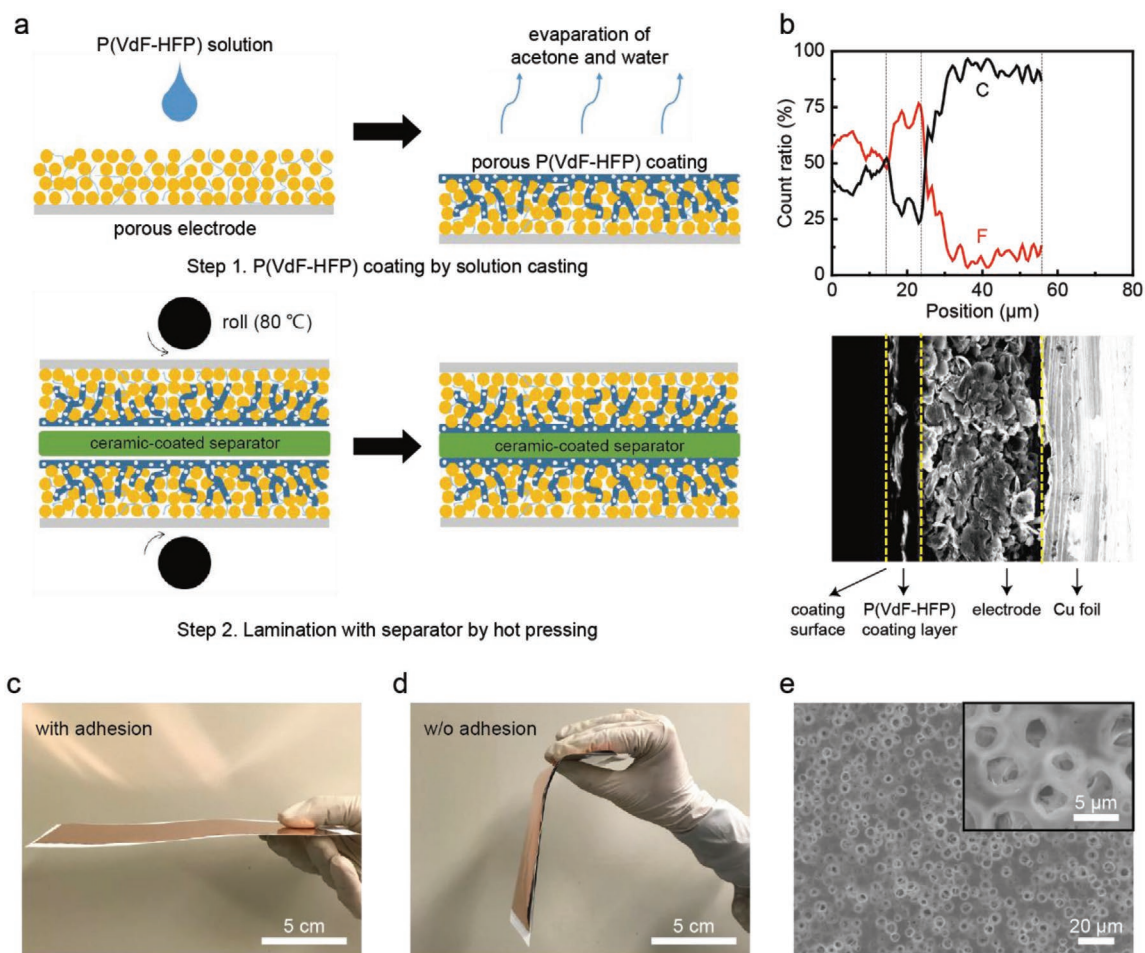


Figure 2. The design and fabrication process of a tree-root-like electrode/separator interface. a) A schematic of the fabrication process of a structural cell with tree-root-like interfaces through hot pressing. b) EDS line scans of C and F in a P(VdF-HFP)-coated graphite, along with an SEM image of the region scanned. The surfaces of P(VdF-HFP) coating, electrode, and Cu current collector are marked with dash lines. c,d) Photos of anode–separator–cathode ensembles c) with and d) without electrode/separator interfacial adhesion. e) Top-view SEM images of a P(VdF-HFP) coating on an NMC electrode after adhesion.

surface and the top 10 μm in the electrode, and also extended deeply into the electrode (15–25 μm). These results indicate that P(VdF-HFP) indeed infiltrated into the porous electrode and formed a tree-root-like structure, which endows strong lamination between a separator and an electrode, and significantly enhances the rigidity of the entire cell. As shown in Figure 2c, a single repeating unit of an anode–separator–cathode trilayer with such interfacial adhesion does not flex by its own weight. In contrast, without such interfacial binding, the trilayer ensemble flexes readily by gravity due to its poor mechanical strength (Figure 2d). In addition, the P(VdF-HFP) layer introduced is highly porous even after hot pressing, which allows ions in the electrolyte to pass readily (Figure 2e). Besides, scanning electron microscopy (SEM) images of a bare NMC electrode, an as-coated NMC electrode before hot pressing, and an as-coated NMC electrode after hot pressing are further presented in Figure S2 (Supporting Information) for a side-by-side comparison.

The P(VdF-HFP)-based interfacial adhesion significantly increases flexural properties of pouch Li-ion cells with

practical sizes. Pouch cells with dimensions of 7.0 cm \times 4.0 cm \times (\approx 2.1) mm ($L \times W \times T$) and 11 graphite/separator/NMC532 repeating units inside were used as samples in mechanical measurements (Figure S1b, Supporting Information), whose configurations are the same as those in FE simulation (Figure 1c). The single-side capacity loadings were 3 and 3.1 mAh cm^{-2} for the NMC cathode and the graphite anode, respectively, and the electrolyte amount was 2.5 g Ah^{-1} . In three-point bending experiments, the cell without the tree-root-like interfacial adhesion shows a low bending force of 0.72 N cm^{-1} at a deflection of 1 mm (Figure 3a), which corresponds to an effective E_f of only 281 MPa, consistent with simulations and literature reports.^[30] The dependence of bending performance on the cell thickness was also studied (Figure S3, Supporting Information). After the tree-root-like adhesion is applied, the bending force is increased by 11.5 times to 9.0 N cm^{-1} at the same deflection, and the corresponding effective E_f is as high as 3.1 GPa. This value, close to epoxy, is among the best results for structural cells with internal strengthening in literature.^[21,34–36] Moreover, the

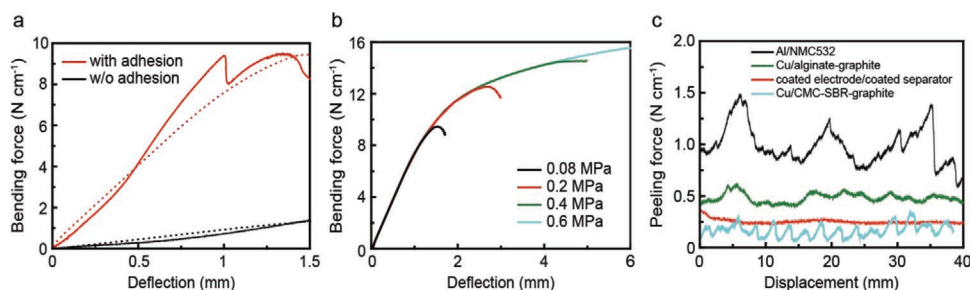


Figure 3. Mechanical properties of structural batteries with proposed interfacial lamination. a) Experimental bending force per width–deflection curves of 2.1 mm thick pouch cells with and without electrode/separator adhesion (solid lines) and corresponding FE simulation results (dotted lines). NMC and graphite electrodes were used in these cells. b) FE simulation of bending force per width–deflection curves of cells with different interfacial adhesion strengths. Adhesion strengths at all electrode/separator and electrode/current collector interfaces are treated to be the same for simplicity. c) 180° peeling-off test results of different interfaces in batteries, including Al/NMC, Cu/CMC–SBR–graphite, P(VdF-HFP)-coated electrode/separator, and Cu/alginate–graphite. The loadings in all electrodes were $\approx 3 \text{ mAh cm}^{-2}$.

processing complexity and extra packaging weights are significantly reduced compared to previously reported strategies for structural batteries. The drop of bending force at 1 mm deflection for the adhered cell is due to imperfection in hot rolling, so areas with weak adhesion tend to fail first, which causes such a sudden drop. The experimental results also align well with FE simulations, further validating our strategy that interfacial adhesion is critical to enhancing the flexural properties of Li-ion cells. Such consistency also shows that simulation is a powerful approach to understand and guide experimental designs of structural batteries.

To better understand the failure mechanism of structural cells with adhered electrode/separator interfaces, a series of FE simulations were performed with the same cell configuration in Figure 1c but with different interfacial adhesion strengths. As the adhesion strength increases from 0.08 to 0.6 MPa, the cell's flexural modulus remains the same, while the bending strength increases significantly (Figure 3b). This is because the interfacial adhesion serves to transfer the shear stress under flexing, and thus it fails when the transferred stress exceeds the adhesion strength. Consequently, the utilization of the electrode/separator adhesion helps increase the flexural modulus of cells, while the reinforcement of the adhesion further improves the bending strength of cells.

Based on the simulation results in Figure 3b, to explore strategies to further strengthen a structural battery, we evaluated the peeling-off strength of various interfaces in a laminated Li-ion cell by a 180° peeling-off test,^[37] followed by strengthening the weakest layer to further improve the strength of the entire full cell. As shown in Figure 3c, While the Al/NMC interface and the coated electrode/separator interface show high peeling-off strengths of ≈ 1.0 and $\approx 0.26 \text{ N cm}^{-1}$, respectively, the Cu/graphite interface has the lowest peeling-off strength of 0.15 N cm^{-1} . To strengthen the weak Cu/graphite interface, and thus the entire cell, we replaced the conventional carboxymethyl cellulose (CMC)–styrene–butadiene rubber (SBR) binder in a graphite electrode with the sodium alginate binder, and the peeling-off strength was significantly enhanced by three times to $\approx 0.5 \text{ N cm}^{-1}$. The stronger adhesion allows for a battery with higher bending strength as illustrated in FE simulation, which provides potential strategies to further enhance the flexing properties of structural batteries.

2.3. Electrochemical Performance

In structural batteries, the electrochemical properties should not be significantly compromised as a trade-off for enhanced mechanical properties. In our strategy, since the extra porous coating is only 5–10 μm in thickness and P(VdF-HFP) has a relatively low density of 1.78 g cm^{-3} , the mass loading of P(VdF-HFP) coating is only $\approx 3.0 \text{ mg cm}^{-2}$ per repeating cell unit, and thus the specific energy of a Li-ion cell is only reduced by 3% due to such a coating (see the Supporting Information for details). This is the smallest reduction in specific energy of structural batteries in literature.^[38] Moreover, the P(VdF-HFP) adhesion layer and alginate binders discussed above are also compatible with other components inside Li-ion cells,^[39,40] and thus the electrochemical performance is expected to remain steady. To demonstrate the stability of electrochemical performance, we tested both half cells and full cells with and without the tree-root-like coating layer. The electrolyte is 1 M lithium difluoro(oxalato)borate (LiDFOB)–0.4 M lithium tetrafluoroborate (LiBF₄) in fluoroethylene carbonate (FEC)–diethyl carbonate (DEC) (1:2, v/v), a recently developed carbonate electrolyte for high-performance lithium batteries.^[41] The areal capacities in electrochemical tests are $\approx 1.0 \text{ mAh cm}^{-2}$, as the purpose of these tests is to demonstrate cycling stability.

Half-cell tests were performed first. Li/NMC532 cells with and without the tree-root-like interfacial adhesion delivered similar specific discharge capacities of 157.3 and 155.9 mAh g^{-1} at C/2, respectively (Figure 4a). The capacity retentions with and without interfacial adhesion are 98.5% and 89.5% after 300 cycles, respectively, and the corresponding average Coulombic efficiencies (CE) are 99.89% and 99.72% from 10th to 300th cycle, respectively. Their voltage profiles indicate that the electrode/separator adhesion does not lead to considerable increase in overpotential during cycling (Figure 4b,c). The electrochemical impedance spectroscopy (EIS) results (Figure S4, Supporting Information) also show that the cell impedance is stable over cycling even with the P(VdF-HFP) coating. The better cycling stability of P(VdF-HFP)-coated NMC532 may come from the good electrolyte swelling properties of P(VdF-HFP) and the passivation of P(VdF-HFP) on the NMC surface.

Similar performance was also observed on the anode side. The Li/graphite half cell with the alginate binder and

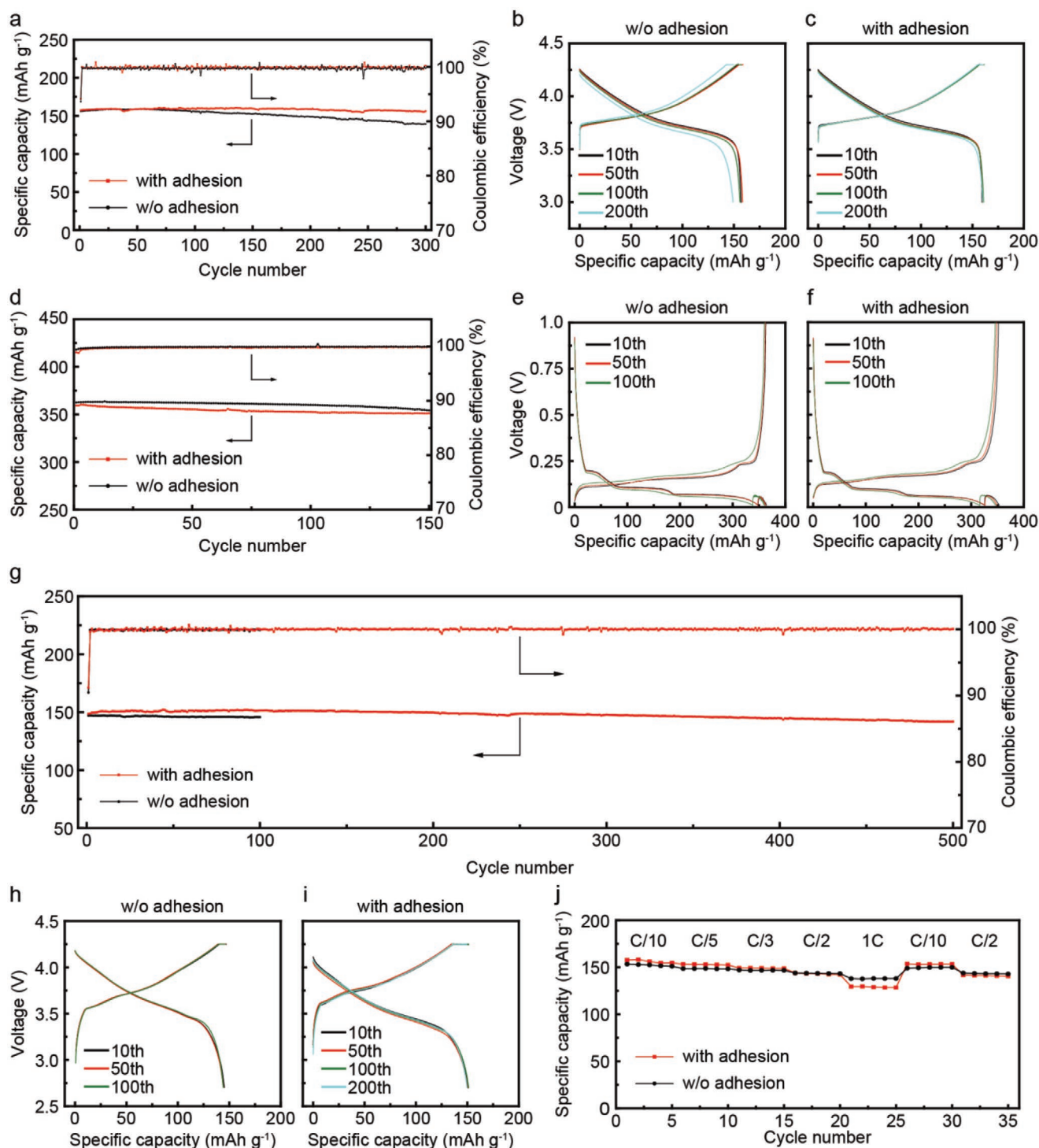


Figure 4. Electrochemical performance of structural batteries with tree-root-like interfacial adhesion and alginate binder. a) Cycling performance of Li/NMC532 half cells with and without electrode/separators adhesion, and b,c) their corresponding voltage profiles for b) without adhesion and c) with adhesion. d) Cycling performance of Li/alginate-graphite half cells with and without electrode/separators adhesion, and e,f) their corresponding voltage profiles for e) without adhesion and f) with adhesion. g) Cycling performance of graphite/NMC532 full cells with and without electrode/separators adhesion. Alginate is used as the binder in the graphite anode. h,i) Corresponding voltage profiles and j) rate performance of graphite/NMC532 full cells. All cells in panels (a)–(j) were first cycled at C/10 for two formation cycles. After the formation cycles, Li/NMC532 cells in panels (a)–(c) and graphite/NMC532 cells in panels (g)–(i) were charged at C/3 with a constant voltage step down to C/20, and discharged at C/2. Li/graphite cells in panels (d)–(f) were lithiated at C/3 to 0.01 V followed by C/20 to 0.01 V, and delithiated to 1.0 V at C/2. In panel (j), the charging rates were always C/3, followed by a CV step to C/20. 1 C is equal to 1.0 mA cm⁻² for all cells.

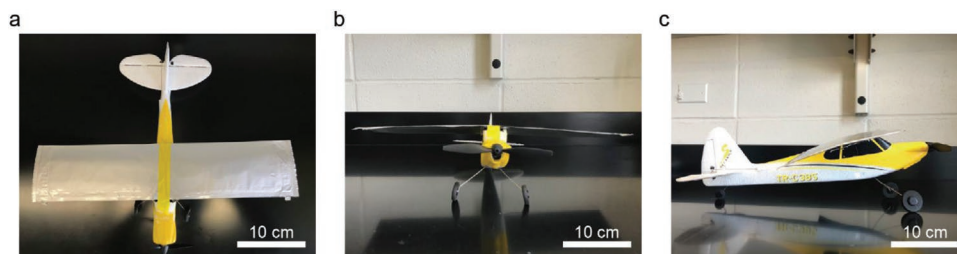


Figure 5. a) Top view, b) front view, and c) side view of an airplane model with laminated pouch cells as “electric wings.” The airplane is in the size of 44 cm × 35 cm × 12 cm ($L \times W \times H$), and it can fly steadily with the wing cells as the only power source (Video S1, Supporting Information). A single-layer electrode is 17.3 cm × 7.5 cm ($L \times W$) in one wing, and one wing can provide a capacity of 780 mAh.

tree-root-like interfacial adhesion delivered a specific discharge capacity of 359 mAh g⁻¹ after two formation cycles and 97.7% retention after 150 cycles (Figure 4d), with an average CE of 99.83% from 10th to 150th cycle. These results are similar to the half cell without the tree-root-like interfacial adhesion, whose specific discharge capacity is 363 mAh g⁻¹ after two formation cycles and has 97.5% retention after 150 cycles (Figure 4d), with an average CE of 99.90% from 10th to 150th cycle. There is also no noticeable difference in their voltage profiles (Figure 4e,f). All data support that the tree-root-like electrode/separator adhesion does not deteriorate the chemical stability of active materials or introduce significant additional overpotentials during cycling.

Based on these positive results, a structural full cell with both the alginate–graphite anode and the NMC532 cathode adhered to the separator was assembled and cycled between 2.7 and 4.25 V. After two formation cycles at $C/10$, the full cell was charged at $C/3$ and discharged at $C/2$ for long-term cycling. The cell showed a specific capacity of 148.6 mAh g⁻¹ in the first cycle after formation cycles, 151.4 mAh g⁻¹ after 100 cycles, and 141.9 mAh g⁻¹ after 500 cycles, corresponding to 95.5% capacity retention. The average CE from 10th to 500th cycle is 99.99% (Figure 4g). The voltage profiles also indicate that the overpotential and internal resistance of the full cell with electrode/separator adhered are stable during cycling, and close to the full cell without such P(VdF-HFP) coating and adhesion (Figure 4h,i). The structural full cell with interfacial adhesion layers also shows a reasonable rate performance. The discharge capacities are 157.7 mAh g⁻¹ at $C/10$, 153.3 mAh g⁻¹ at $C/5$, 149.2 mAh g⁻¹ at $C/3$, 144 mAh g⁻¹ at $C/2$, and 129.5 mAh g⁻¹ at 1 C, close to those in a cell without tree-root-like interfacial adhesion (Figure 4i). These results demonstrate that cells with the proposed tree-root-like adhesion have reasonable electrochemical performance and satisfactory long-term stability, and remarkably enhanced mechanical properties.

2.4. Prototype Demonstration of “Electric Wings”

To demonstrate practical applications of the proposed strategy in real devices, we replaced the wings of an aircraft model by two laminated structural pouch cells with dimensions of 23 cm × 9.0 cm × 0.6 mm ($L \times W \times T$) (Figure 5). Each cell has a capacity of 780 mAh with two 3 mAh cm⁻² anode–separator–cathode units, and the aircraft was solely powered by these “electric wings.” With laminated cells, the aircraft model

can fly steadily and smoothly, which benefits from the stiffness and lightness of the proposed structural batteries (Video S1, Supporting Information). In contrast, with conventional cells without interfacial lamination as wings, the aircraft model with the same weight falls soon after being thrown to the sky, due to the much weaker strength of the wings (Video S1, Supporting Information). Such distinctly different behaviors demonstrate the superiority of structural energy storage for lightweighting aerial vehicles.

3. Summary

In conclusion, we demonstrated a tree-root-inspired interfacial adhesion between battery electrodes and separators, which increases the bending modulus of batteries by 11 times to 3.1 GPa at appreciable deflections. FE simulations were conducted to reveal the enhancement mechanism that this adhesion eliminates the relative sliding between different layers and allows all layers to share a common neutral axis when the battery is bent, which validates experimental results. Therefore, the load transfer is more efficient through the battery, and better flexural properties are realized. Due to the small thickness of the adhesion layer, this strategy only reduces the specific energy of batteries by 3%, which is the smallest reduction reported in structural batteries. Moreover, this strategy does not affect electrochemical performance significantly, and satisfactory specific capacities and capacity retentions were observed. A graphite/NMC532 full cell with adhered electrode/separator interfaces delivered a specific capacity of 148.6 mAh g⁻¹ at $C/2$, and a high capacity retention of 95.5% after 500 cycles. All these properties allow such a structural cell to independently power unmanned aerial vehicle models as electric wings. These results declare that with this rational interfacial design, the flexing performance of batteries can be vastly increased by making full use of the intrinsic strength of current collectors with electrochemical properties being maintained. The adaptability in this strategy leaves itself much space for further amelioration and combination with other strategies like mechanically stronger battery materials.

Supporting Information

Supporting Information is available from the Wiley Online Library or from the author.

Acknowledgements

The authors appreciate the funding support from AFOSR (FA9550-20-1-0233) and helpful discussions about simulations with Juner Zhu and Wei Li at MIT.

Conflict of Interest

The authors declare no conflict of interest.

Data Availability Statement

The data that support the findings of this study are available from the corresponding author upon reasonable request.

Keywords

finite element simulation, interfacial design, specific energy, structural energy storage

Received: March 29, 2021

Revised: April 26, 2021

Published online:

- [1] M. T. McDowell, S. W. Lee, W. D. Nix, Y. Cui, *Adv. Mater.* **2013**, *25*, 4966.
- [2] W. Li, H. Yao, K. Yan, G. Zheng, Z. Liang, Y.-M. Chiang, Y. Cui, *Nat. Commun.* **2015**, *6*, 7436.
- [3] K. Zhao, M. Pharr, J. J. Vlassak, Z. Suo, *J. Appl. Phys.* **2010**, *108*, 073517.
- [4] K. Kang, Y. S. Meng, J. Bréger, C. P. Grey, G. Ceder, *Science* **2006**, *311*, 977.
- [5] J. Liu, Z. Bao, Y. Cui, E. J. Dufek, J. B. Goodenough, P. Khalifah, Q. Li, B. Y. Liaw, P. Liu, A. Manthiram, Y. S. Meng, V. R. Subramanian, M. F. Toney, V. V. Viswanathan, M. S. Whittingham, J. Xiao, W. Xu, J. Yang, X.-Q. Yang, J.-G. Zhang, *Nat. Energy* **2019**, *4*, 180.
- [6] C. Niu, H. Lee, S. Chen, Q. Li, J. Du, W. Xu, J.-G. Zhang, M. S. Whittingham, J. Xiao, J. Liu, *Nat. Energy* **2019**, *4*, 551.
- [7] L. Hu, K. Xu, *Proc. Natl. Acad. Sci. USA* **2014**, *111*, 3205.
- [8] L. Suo, O. Borodin, T. Gao, M. Olguin, J. Ho, X. Fan, C. Luo, C. Wang, K. Xu, *Science* **2015**, *350*, 938.
- [9] A. Li, X. Liao, H. Zhang, L. Shi, P. Wang, Q. Cheng, J. Borovilas, Z. Li, W. Huang, Z. Fu, M. Dontigny, K. Zaghbi, K. Myers, X. Chuan, X. Chen, Y. Yang, *Adv. Mater.* **2020**, *32*, 1905517.
- [10] E. S. Greenhalgh, J. Ankersen, L. E. Asp, A. Bismarck, Q. P. V. Fontana, M. Houille, G. Kalinka, A. Kucernak, M. Mistry, S. Nguyen, H. Qian, M. S. P. Shaffer, N. Shirshova, J. H. G. Steinke, M. Wienrich, *J. Compos. Mater.* **2014**, *49*, 1823.
- [11] Y. Wang, C. Peng, W. Zhang, *Appl. Therm. Eng.* **2015**, *78*, 209.
- [12] W. Huang, P. Wang, X. Liao, Y. Chen, J. Borovilas, T. Jin, A. Li, Q. Cheng, Y. Zhang, H. Zhai, A. Chitu, Z. Shan, Y. Yang, *Energy Storage Mater.* **2020**, *33*, 416.
- [13] A. S. Hollinger, D. R. McAnallen, M. T. Brockett, S. C. DeLaney, J. Ma, C. D. Rahn, *Int. J. Energy Res.* **2020**, *44*, 560.
- [14] L. E. Asp, M. Johansson, G. Lindbergh, J. Xu, D. Zenkert, *Funct. Compos. Struct.* **2019**, *1*, 042001.
- [15] W. Johannisson, D. Zenkert, G. Lindbergh, *Multifunct. Mater.* **2019**, *2*, 035002.
- [16] Y. C. Zhang, J. Ma, A. K. Singh, L. Cao, J. Seo, C. D. Rahn, C. E. Bakis, M. A. Hickner, *J. Intell. Mater. Syst. Struct.* **2017**, *28*, 1603.
- [17] S. C. Roberts, G. S. Aglietti, *Acta Astronaut.* **2010**, *67*, 424.
- [18] T. Pereira, Z. H. Guo, S. Nieh, J. Arias, H. T. Hahn, *Compos. Sci. Technol.* **2008**, *68*, 1935.
- [19] L. E. Asp, E. S. Greenhalgh, *Compos. Sci. Technol.* **2014**, *101*, 41.
- [20] J. F. Snyder, E. L. Wong, C. W. Hubbard, *J. Electrochem. Soc.* **2009**, *156*, A215.
- [21] P. Liu, E. Sherman, A. Jacobsen, *J. Power Sources* **2009**, *189*, 646.
- [22] K. Moyer, C. Meng, B. Marshall, O. Assal, J. Eaves, D. Perez, R. Karkkainen, L. Roberson, C. L. Pint, *Energy Storage Mater.* **2020**, *24*, 676.
- [23] G. Fredi, S. Jeschke, A. Boulaoued, J. Wallenstein, M. Rashidi, F. Liu, R. Harnden, D. Zenkert, J. Hagberg, G. Lindbergh, P. Johansson, L. Stievano, L. E. Asp, *Multifunct. Mater.* **2018**, *1*, 015003.
- [24] H. Li, S. Wang, M. Feng, J. Yang, B. Zhang, *J. Mater. Sci.* **2018**, *53*, 11607.
- [25] S. Leijonmarck, T. Carlson, G. Lindbergh, L. E. Asp, H. Maples, A. Bismarck, *Compos. Sci. Technol.* **2013**, *89*, 149.
- [26] J. Hagberg, S. Leijonmarck, G. Lindbergh, *J. Electrochem. Soc.* **2016**, *163*, A1790.
- [27] E. Jacques, M. H. Kjell, D. Zenkert, G. Lindbergh, *Carbon* **2014**, *68*, 725.
- [28] M. H. Kjell, E. Jacques, D. Zenkert, M. Behm, G. Lindbergh, *J. Electrochem. Soc.* **2011**, *158*, A1455.
- [29] A. Patel, K. Wilcox, Z. Li, I. George, R. Juneja, C. Lollar, S. Lazar, J. Grunlan, W. E. Tenhaeff, J. L. Lutkenhaus, *ACS Appl. Mater. Interfaces* **2020**, *12*, 25756.
- [30] P. Ladpli, R. Nardari, F. Kopsaftopoulos, F. K. Chang, *J. Power Sources* **2019**, *414*, 517.
- [31] W. Li, J. Zhu, Y. Xia, M. B. Gorji, T. Wierzbicki, *Joule* **2019**, *3*, 2703.
- [32] L. E. Asp, K. Bouton, D. Carlstedt, S. Duan, R. Harnden, W. Johannisson, M. Johansen, M. K. G. Johansson, G. Lindbergh, F. Liu, K. Peuvot, L. M. Schneider, J. Xu, D. Zenkert, *Adv. Energy Sustainability Res.* **2021**, *2*, 2000093.
- [33] J. Mandal, Y. Fu, A. C. Overvig, M. Jia, K. Sun, N. N. Shi, H. Zhou, X. Xiao, N. Yu, Y. Yang, *Science* **2018**, *362*, 315.
- [34] A. Thakur, X. Dong, *Manuf. Lett.* **2020**, *24*, 1.
- [35] K. Moyer, C. Meng, B. Marshall, O. Assal, J. Eaves, D. Perez, R. Karkkainen, L. Roberson, C. L. Pint, *Energy Storage Mater.* **2020**, *24*, 676.
- [36] J. P. Thomas, M. A. Qidwai, *Acta Mater.* **2004**, *52*, 2155.
- [37] M.-H. Ryou, J. Kim, I. Lee, S. Kim, Y. K. Jeong, S. Hong, J. H. Ryu, T.-S. Kim, J.-K. Park, H. Lee, J. W. Choi, *Adv. Mater.* **2013**, *25*, 1571.
- [38] B. J. Hopkins, J. W. Long, D. R. Rolison, J. F. Parker, *Joule* **2020**, *4*, 2240.
- [39] I. Kovalenko, B. Zdyrko, A. Magasinski, B. Hertzberg, Z. Milicev, R. Burtovyy, I. Luzinov, G. Yushin, *Science* **2011**, *334*, 75.
- [40] T. Jin, Y. Wang, Z. Hui, B. Qie, A. Li, D. Paley, B. Xu, X. Wang, A. Chitu, H. Zhai, T. Gong, Y. Yang, *ACS Appl. Mater. Interfaces* **2019**, *11*, 17333.
- [41] C. Martin, M. Genovese, A. J. Louli, R. Weber, J. R. Dahn, *Joule* **2020**, *4*, 1296.